3-1-2001

Gravity Wave Propagation Directions Inferred from Satellite Observations including Smearing Effects

Jason S. Brown
Clemson University

Michael P. Hickey Ph.D.
Embry-Riddle Aeronautical University, hicke0b5@erau.edu

JOURNAL OF GEOPHYSICAL RESEARCH, VOL. 106, NO. A3, PAGES 3631-3643, MARCH 1, 2001

Gravity wave propagation directions inferred from satellite observations including smearing effects

Jason S. Brown and Michael P. Hickey

Department of Physics and Astronomy, Clemson University, Clemson, South Carolina

Abstract. We simulate space-based, sublimb viewing observations of airglow brightness fluctuations caused by atmospheric gravity wave interactions with the O_2 atmospheric airglow, and we demonstrate that because of the geometry associated with such observations, the brightness fluctuations observed for the optically thick 0-0 band emission will always appear stronger for waves traveling toward the observer (the satellite). The effect should be most noticeable for waves having relatively small vertical wavelengths (~10 km) and horizontal wavelengths of 50 km or greater. For waves of short (~100 km) horizontal wavelength, the brightness fluctuation anisotropy with respect to viewing direction may also be evident in the optically thin 0-1 band emission. We demonstrate that the waves will be observable despite the fact that an instrument requires a certain finite integration time to achieve a desired signal-to-noise ratio. Therefore the 180° ambiguity in wave propagation direction associated with space-based observations may be eliminated for waves of small vertical wavelength that are dissipating in the upper mesosphere and lower thermosphere. It is these same waves that may be expected to be important to the energy and momentum budgets of the mesosphere/lower thermosphere region.

1. Introduction

It has become clear that in order to improve our understanding of the influences of atmospheric gravity waves on the mesosphere/lower thermosphere (MLT) region momentum and energy budgets, global characterization of the waves acquired through long-term, global observations using one or more suitably instrumented satellites is required. Because typical satellite orbital speeds (~8 km s^{-1}) greatly exceed typical MLT region gravity wave phase speeds (≤100 m s^{-1}), the wave system appears stationary to satellites. Therefore, even when the azimuthal orientation of the phase fronts can be determined from such observations; there exists a 180° ambiguity in the inferred direction of wave propagation. Resolving this ambiguity is critical to the determination of gravity wave momentum forcing of the mean state.

This ambiguity in propagation direction can be eliminated by combining coincident ground-based observations with satellite observations, however, such an approach has obvious limitations. First, the geographical distribution of the limited number of suitable ground stations is not well suited for such correlative studies. Two thirds of the ocean-covered Earth is not accessible to such sites, which would bias the inferred wave spectra [e.g., *Fritts et al.*, 1989]. Second, ground-based optical observations are limited by viewing conditions (note that radars do not suffer from this limitation). Therefore it would be highly desirable to develop a method of removing the directional ambiguity using the satellite data alone.

Several observations have been made of nightglow fluctuations from space-based experiments [e.g., *Swenson et al.*, 1989; *Ross et al.*, 1992; *Mende et al.*, 1994; *Hays et al.*, 1994; *Armstrong et al.*, 1995], and Upper Atmosphere Research Satellite (UARS) observations have revealed wave structures with horizontal wavelengths as small as 20 km [*Hays et al.*, 1994; *Kafkalidis et al.*, 1996]. Unfortunately, NASA's Thermosphere, Ionosphere, and Mesosphere Energetics and Dynamics (TIMED) satellite will not be making gravity wave measurements. Some of the earlier wave measurements will be described later in the discussion section.

The objective of this study is to demonstrate that the ambiguity associated with the gravity wave propagation direction can be alleviated for waves that are likely to be important to the energy and momentum budgets of the MLT region. We do so using a gravity wave model and a chemistry/airglow fluctuation model to simulate satellite observations of airglow perturbations, as described in the next section. Specifically, we simulate sublimb forward viewing observations of gravity waves that exist in the airglow in some region ahead of the spacecraft and backward viewing observations of the same region of the airglow at some later time. Results are presented for four different categories of waves in section 3, and discussions and conclusions follow in sections 4 and 5, respectively.

2. Method

The models used here are a linear, steady state full-wave model describing the wave dynamics and a linear, steady state chemistry model describing airglow fluctuations subject to wave perturbations. These models have been previously used to simulate gravity wave-driven fluctuations of the O I 5577 nightglow [*Hickey et al.*, 1997, 1998; *Schubert et al.*, 1999] and the O_2 atmospheric 0-1 band nightglow [*Hickey and Walterscheid*, 1999]. We additionally simulate the 0-0 band O_2 atmospheric nightglow by incorporating the effects of self-absorption (described below) and also using the radiation transition probability for the 0-1 band. The latter assumption

Paper number 2000JA000272.
0148-0227/01/2000JA000272$09.00

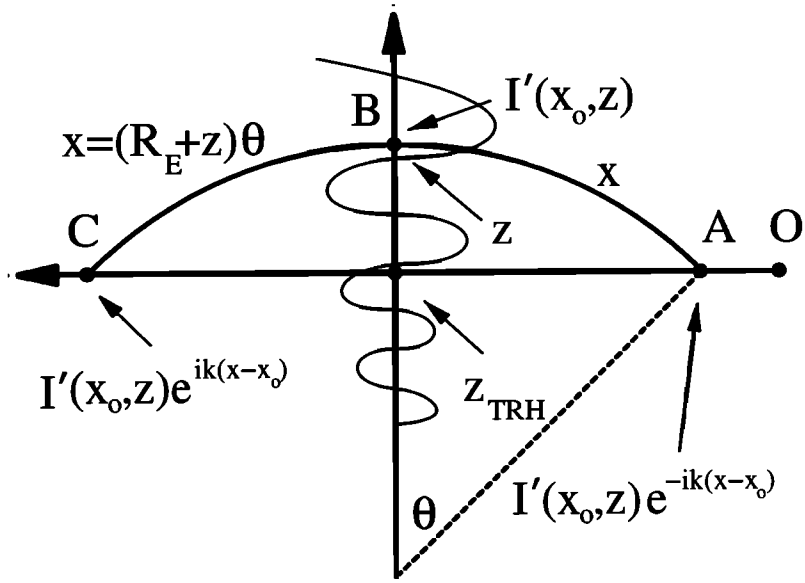

Figure 1. Schematic (not to scale) showing the geometry for wave propagation in a spherical atmosphere as viewed from a satellite. Points A, B, and C all lie at the same altitude z, and the line of sight (tangent ray path) extends from the observer (at O) through A, C, and the tangent ray point at height z_{TRH}. The arc length x and the horizontal wavenumber k are used to define the perturbations at A and C in terms of that at B.

leads to mean volumetric emission rates (VER) for the 0-0 band that are the same as those of the 0-1 band, when in fact it is known that the 0-0 band VER is much greater than the 0-1 band VER [*Torr et al.*, 1985]. This should not significantly influence our results because we are interested in determining relative airglow brightness fluctuations, which are independent of absolute brightness.

Application of these ground-based simulation models to the simulation of space-based observations of airglow variations is facilitated by calculating the total (mean plus wave perturbation) VER as a function of altitude (z) for some arbitrary horizontal position (x). We therefore write $I(x,z) = \bar{I}(z) + I'(x,z)$, where I represents airglow VER, the overbar denotes the unperturbed mean state, and the prime denotes a linear perturbation about the mean state. Our full-wave/airglow fluctuation model provides $I'(x_o,z)$ at the reference position x_o. Assuming a spherical Earth, a horizontally homogeneous mean state, and also that the wave variations in the horizontal direction are purely harmonic with horizontal wavenumber k allows us to determine the VER at any position as $I(x,z) = \bar{I}(z) + I'(x_o,z)\exp[-ik(x-x_o)]$. Simulation of the airglow brightness then proceeds by integration of this quantity along a specified tangent ray path. The coordinates in our Cartesian coordinate system (x,z) are transformed to a spherical coordinate system (r,θ) using $r = R_E + z$ and $x = r\theta$, where R_E is the Earth's radius. The validity of this transformation for gravity wave propagation is supported by the work of *Francis* [1972], who has shown that large-scale gravity waves are refracted around the spherical Earth by the effects of gravity gradients. The geometry for such observations is shown in Figure 1.

The dynamical/airglow model is used to simulate space-based observations of gravity wave-driven O_2 atmospheric 0-0 and 0-1 band airglow fluctuations. The model output VER is interpolated using a smoothing cubic spline. The upper limit of integration along the line of sight corresponds to an altitude of 130 km and encompasses the relevant airglow region of the atmosphere. For each calculation a 400-point Gauss-Legendre quadrature scheme is used to integrate the emission rate along the constrained line of sight, which is sufficiently accurate to handle the wide range of wave parameters responsible for driving a given airglow response. The direction of viewing is determined relative to the direction of motion of the observer. "Forward viewing" ("backward viewing") is defined as viewing along (opposite to) the direction of the observer's motion. The total brightness is calculated as a function of satellite position, and then averaging over one wavelength provides the mean brightness. Half of the difference between these two then provides the brightness perturbation amplitude. A similar procedure could also be applied in the analysis of actual satellite data.

For the optically thick O_2 0-0 band atmospheric emission, the self-absorption is calculated using the Lambert-Beer law and a band-averaged optical depth (τ) given by *Wallace and Hunten* [1968], namely, $\tau = 1.6\times10^{-22}[O_2](245/T)$, where T is temperature. Values of T and $[O_2]$ are the same mean-state values as those used in the full-wave model and defined using the MSIS-90 model [*Hedin*, 1991]. These data are also interpolated using a smoothing cubic spline. The amount of absorption is determined at each Gauss-Legendre abscissa, which represents a point along the line of sight. For a given abscissa, the amount of absorption is determined by the integral of the optical depth along the line of sight from this abscissa to the observer. The trapezoidal rule is used for this integration (with an accuracy of approximately four decimal places) and is only implemented between adjacent abscissae to avoid multiple calculations of the same quantities. During final quadrature to obtain the total integrated intensity, each absorption term is multiplied by the value of the VER (the integrand) at a given abscissa. The final quadrature yields the brightness (for both forward and backward viewing) of the 0-0 band O_2 atmospheric emission. The mean VER of the O_2

atmospheric emission used here peaks at about 91.5 km altitude with a value of 2.76 x 10^8 photons m^{-3} s^{-1} and has a full width at half maximum of about 10 km.

We also consider the fact that in order to perform a single measurement, an instrument requires a certain finite integration time to achieve a desired signal-to-noise ratio. The integration process will produce smearing, which will wash out the smaller-scale waves in space-based airglow observations. Typical nadir pointing instruments require integration times greater than about 20 s to obtain useable signal-to-noise ratios. However, the signal strength depends on the slant path, being largest for limb viewing and smallest for nadir viewing. We have calculated and compared the brightness obtained (in the absence of waves) for nadir viewing and for sublimb viewing with a tangent ray height of 40 km and found that the brightness for the latter is a factor of approximately 16 times greater than that of the former. This suggests that space-based instruments viewing the sublimb should be able to receive strong enough signals to allow the use of integration times as short as ~2 s. As an example, *Mende et al.* [1994] performed topside measurements of the O_2 atmospheric nightglow using an image intensified charge-coupled device (CCD) detector looking slightly below the limb. Typically, 1-s exposures were taken, allowing them to identify gravity waves having horizontal wavelengths of 50-100 km. More details are provided in the discussion. Additionally, instruments can be operated in so-called "staring modes," wherein the same region of the airglow is sampled during the course of the satellite motion. This tends to reduce smearing effects. Also, because airglow brightness differs between the different airglow emissions, the integration times required for measurements will vary from one emission to another. A good comparison of the different airglow emissions is given by *Chamberlain* [1995].

Typically, integration times of a few seconds are required, which will smear waves having horizontal wavelengths of ~50 km or less. This estimate is based on a 2.5-s integration time, the requirement of at least two such measurements to resolve the wave, and assuming a satellite speed of about 8 km s^{-1}. To account for such averaging, integrated airglow intensity amplitudes were obtained using a 5-s integration time. The resulting averages were then interpolated with a smoothing spline from which new brightness amplitudes were determined. As will be noted in section 3, the effect of smearing is small for short-wavelength waves (~100 km) and is negligible for long-wavelength ($\geq$ 100 km) waves.

3. Results

We consider gravity waves having phase speeds in the range 15-150 m s^{-1} and with two different horizontal wavelengths (100 and 1000 km). The range of vertical wavelengths at the altitude of the peak in the O_2 atmospheric airglow VER is approximately 10-100 km for phase velocities in the range of 15-150 m s^{-1}. With fairly modest values of eddy diffusion used in our model (peak values of about 200 m^2 s^{-1} at 90 km altitude) and with the additional effects of molecular diffusion, these waves achieve maximum amplitudes at different altitudes (designated z_{peak}), as provided in Figure 2a. The actual values of temperature amplitude we used (see Figure 2b) were based on the requirement that the minimum gradient of total potential temperature be zero [*Orlanski and Bryan*, 1969]. However, for waves with phase velocities larger than about 30 m s^{-1} that achieve maximum amplitudes well into the thermosphere, this procedure produced unrealistically large wave amplitudes. For these waves, if the perturbation temperatures (T') exceeded 10% of the mean temperature ($\overline{T}$) at any altitude greater than 30 km, we set maximum temperature amplitudes equal to 10% of the mean at z_{peak}. This ensured that these waves have linear amplitudes everywhere (i.e., $|T'|/\overline{T} = 0.1$). Consequently, waves satisfying this latter condition have significantly smaller amplitudes than those satisfying the Orlanski-Bryan criterion within the airglow region (by a factor of between about 5 and 10). The Orlanski-Bryan condition was applied for waves of phase speed <35 m s^{-1} and <30 m s^{-1} for 100 km and 1000 km horizontal wavelengths, respectively. For faster waves, we set $|T'|/\overline{T} = 0.1$ at altitude z_{peak}

We consider space-based observations using tangent ray heights (z_{TRH}) of 40 and 85 km. For the optically thin emission the airglow emission from the far side of the tangent ray point will make a significant contribution to the total observed brightness. However, for z_{TRH} =40 km, this "far" region will lie at a significant distance from the foreground region (~1600 km). Therefore, in the case of short (100 km) horizontal wavelength waves we consider, it would be unlikely that a given gravity wave would exist simultaneously at both locations. This is because gravity waves are primarily a local phenomenon and correlation distances are not usually as large as 16 wavelengths. (Ducted waves are a different matter, but these are not considered here.) Accordingly, we consider only the contribution of the foreground emission when calculating the brightness fluctuations for the optically thin emission and for the 100 km horizontal wavelength waves. We include the contributions from both regions (foreground and background) when we calculate the mean brightness and also when we calculate brightness fluctuations for the 1000 km horizontal wavelength waves. Also, as we increase z_{TRH}, the distance between disturbances in the foreground and background regions becomes smaller (see discussion below), and it is more likely that wave disturbances in these two regions would be correlated. Therefore, for the z_{TRH} =85 km results, we include the contributions from the foreground and background regions.

Figure 3a is a schematic showing the slope (at angle ϕ) of gravity wave phase fronts (solid lines) in a spherical atmosphere with respect to the local vertical coordinate (short-dashed lines) and the tangent ray paths (dash-dotted lines). The satellite initially observes an airglow disturbance at time t while forward viewing, and at a later time $t+\delta t$, it observes the same airglow disturbance while backward viewing. The apparent wavelengths as seen along the line of sight at the two observing times are represented by the line segments $\overline{AB}$ and $\overline{CD}$, respectively. In general, the apparent wavelengths for forward and backward viewing are not equal. This is a geometry effect, and it arises for wave propagation on a spherical Earth because the phase fronts for waves of short vertical wavelength (those with small phase speeds) have a significant tilt from the vertical. The apparent wavelength will always be greater when viewing waves propagating toward the observer (in our case, $\overline{CD} > \overline{AB}$). For waves having large vertical wavelengths (for which $\phi \approx 0$), the importance of this geometry effect diminishes because the phase fronts for such waves are almost vertical and the perturbation VER is therefore approximately symmetrical about the tangent ray point.

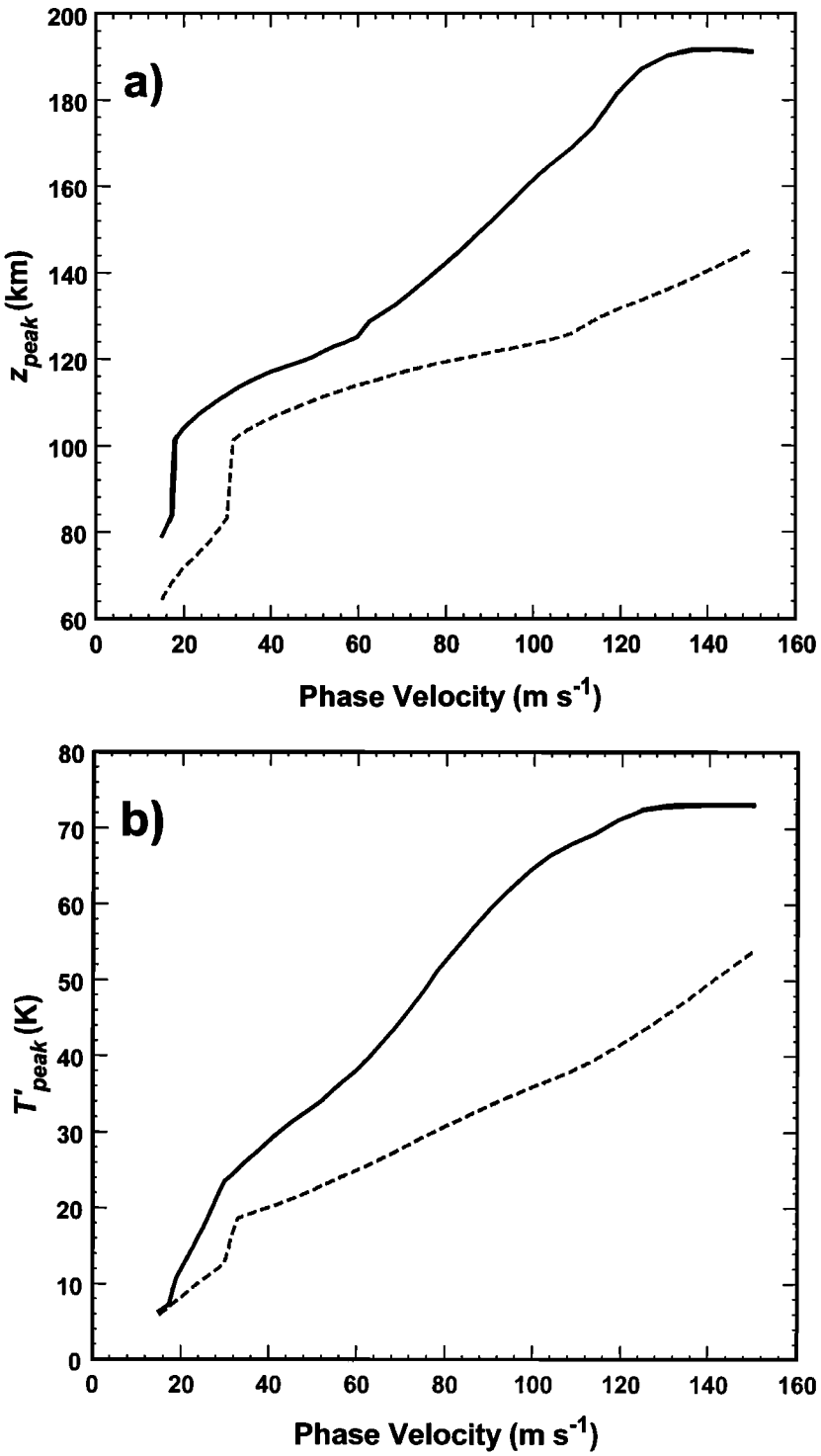

Figure 2. (a) The peak altitude of the temperature fluctuations (z_{peak}) plotted as a function of phase speed for the waves used in our simulations. The solid (dashed) curve is z_{peak} for waves of 100 km (1000 km) horizontal wavelength. (b) The corresponding value of the maximum temperature perturbation (T'_{peak}) as a function of phase speed. The solid (dashed) curve is T'_{peak} for waves of 100 km (1000 km) horizontal wavelength.

Figure 3b represents the case for satellite observations made at large z_{TRH} where the line of sight is approximately equivalent for both forward and backward viewing. For large z_{TRH}, the viewing angle is shallow enough that the VER along the line of sight is centered about and lies close to the tangent ray point Q (see Figure 4). Therefore any disturbance in airglow brightness measured at large z_{TRH} is most probably a result of VER fluctuations that are correlated on either side of Q. In the case of the optically thin 0-1 band emission, for example, we should expect no difference between forward and backward viewing because the VER is equivalent in both viewing directions, regardless of the differences in apparent wavelengths $\overline{AB}$ and $\overline{CD}$. For the optically thick 0-0 band emission, however, the VER will not be symmetrical on either

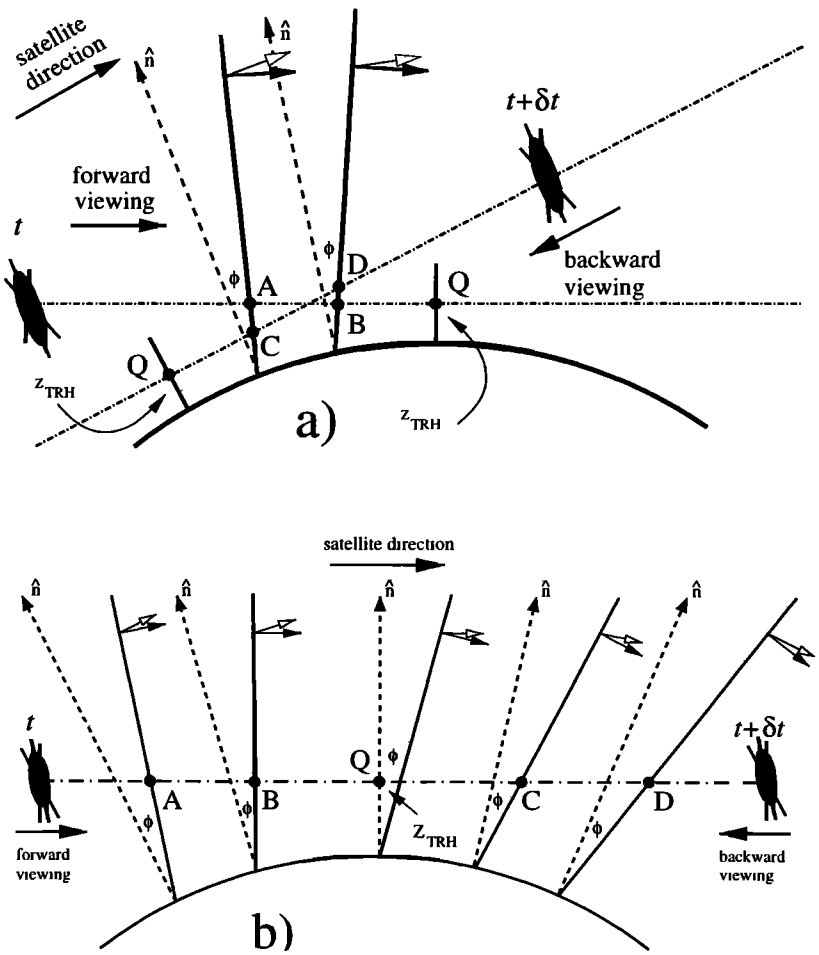

Figure 3. (a) Schematic (not to scale) representing the difference associated with viewing direction of an airglow disturbance. The solid lines represent lines of constant phase at angle ϕ relative to a local vertical coordinate (dashed lines). Arrows represent the total (solid) and horizontal (open) wavenumber vectors. The dash-dotted lines represent the tangent ray paths for forward (at time t) and backward (at time $t+\delta t$) viewing for a given tangent ray height z_{TRH}. The apparent wavelengths represented by the distances $\overline{AB}$ (for forward viewing) and $\overline{CD}$ (backward viewing) are not equal ($\overline{CD} > \overline{AB}$), leading to increased destructive interference and a smaller brightness fluctuation for forward viewing. (b) Same as Figure 3a but for large z_{TRH}. The volume emission rate (VER) is necessarily correlated about tangent ray point Q, so differences in $\overline{AB}$ and $\overline{CD}$ will not affect brightness fluctuations for the optically thin 0-1 band emission.

side of Q due to self-absorption. Therefore brightness fluctuations will appear larger for backward viewing because $\overline{CD} > \overline{AB}$.

Figure 4 shows the perturbation VER plotted as a function of distance along the line of sight for a wave with a horizontal wavelength of 100 km and a phase speed of 30 m s^{-1} for z_{TRH} =40 km and z_{TRH}=85 km. These results were obtained assuming that the waves and satellite are moving in the same direction. Accordingly, negative and positive distances correspond to forward and backward viewing, respectively. The mean VER (not shown) is symmetrical about the tangent ray point (x=0), but the perturbation VER is not. This asymmetry is most evident for z_{TRH} = 40 km, where it can be clearly seen that the apparent wavelength is much smaller for forward viewing than for backward viewing. For z_{TRH}=85 km the perturbation VER is centered about and lies close to the tangent ray point and does not exhibit the same degree of asymmetry with respect to the distance from the tangent ray point as for the z_{TRH} =40 km case. Notice that the number of oscillations in the VER for z_{TRH}=85 km exceeds that of the VER for z_{TRH}=40 km. In this case, we should expect less destructive interference and stronger brightness fluctuation amplitudes for 100 km horizontal wavelength waves viewed at z_{TRH}=40 km.

Integration of the total VER along the tangent ray provides the observed brightness ($\overline{B} + B'$), where $\overline{B}$ and B' are the undisturbed and perturbation brightness, respectively. Values of $B'/\overline{B}$ for both forward and backward viewing are presented for the four cases as a function of phase speed in Figure 5. For z_{TRH}=40 km, $\overline{B}$ is about 40.9 and 20.2 kR for the optically thin and optically thick emissions, respectively. For z_{TRH}=85 km, $\overline{B}$ is about 122.2 and 103.8 kR for the optically thin and optically thick emissions, respectively. The mean brightness values reflect the dependence of absorption on tangent ray height. For steep viewing angles (z_{TRH} = 40 km), O_2 absorption attenuates essentially all contributions to the mean brightness on the far side of the tangent ray point. Additionally, the path length intersecting the airglow region is shorter for the lower tangent ray height, resulting in the

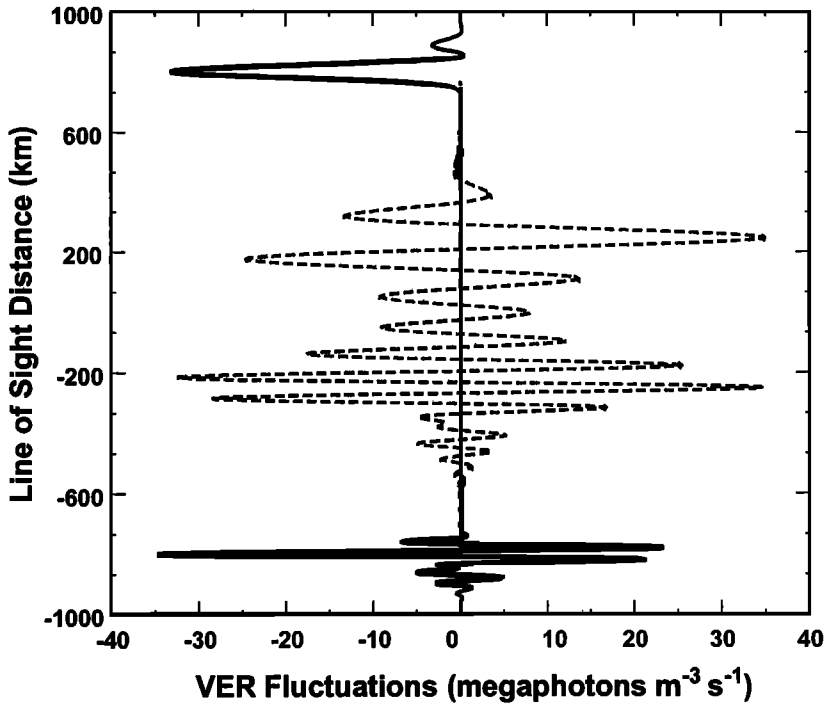

Figure 4. The perturbation VER plotted as a function of distance along the line of sight for a wave of 100 km horizontal wavelength and 30 m s^{-1} phase velocity. Negative and positive distances correspond to forward and backward viewing, respectively. Note the apparent compression of the wavelength along the tangent ray for forward viewing. The solid and dashed curves correspond to z_{TRH} equal to 40 km and 85 km, respectively.

smaller undisturbed brightness. For shallower viewing angles (z_{TRH} = 85 km) the effects of self-absorption are not as pronounced, because the O_2 concentration is smaller along this line of sight.

For all cases, $B'/\overline{B}$ for the optically thick 0-0 band emission is greater for viewing in the backward direction relative to the value obtained for viewing in the forward direction. The effect is most pronounced for phase speeds less than about 100 m s^{-1}. In fact, for some cases, waves from the forward direction would be unobservable because the apparent wavelength of the wave (along the line of sight) is very small for this viewing direction.

Figure 5a shows $B'/\overline{B}$ for the 100 km horizontal wavelength wave at z_{TRH} = 40 km as a function of phase speed. Here there is a significant difference in brightness for forward versus backward viewing. For forward viewing, the waves are completely unobservable at all phase speeds, but backward viewing values should be clearly observable ($B'/\overline{B} \geq 5\%$) in a phase velocity range of approximately 15-40 m s^{-1}. Our assumption that 5% airglow variations due to gravity waves would be observable is discussed in section 4. For backward viewing, the maximum in $B'/\overline{B}$ occurs at a phase speed of about 25 m s^{-1}, where $B'/\overline{B}$ is about 11% and 5% for the 0-0 and 0-1 bands, respectively. The maximum in $B'/\overline{B}$ also corresponds approximately to the maximum in the difference in $B'/\overline{B}$ for forward versus backward viewing (which is approximately a factor of 25 there). For both forward and backward viewing, the optically thick emission has a larger value of $B'/\overline{B}$ by a factor of approximately 2 for phase velocities greater than about 15 m s^{-1} as compared with the 0-1 band emission. As discussed previously, the 100 km horizontal wavelength waves are expected to be uncorrelated about the tangent ray point, and so VER fluctuations originating from the far side of the tangent ray point are not included for observations made at z_{TRH} = 40 km. Note, however, that the undisturbed VER originating from the far side of the tangent ray point will contribute to the observed brightness. This exclusion leads to the difference in brightness for forward and backward viewing for the optically thin emission. However, in the case of the optically thick emission (for z_{TRH} = 40 km), all emissions emanating from the far side of the tangent ray point will be absorbed before reaching the observer. Therefore the value of $B'/\overline{B}$ is determined solely by processes occurring on the near side of the tangent ray point. Because $\overline{B}$ for the optically thick emission is approximately half that for the optically thin emission, while B' for the two emissions are approximately equal (assuming no disturbance on the far side of the tangent ray point), then $B'/\overline{B}$ for the optically thick emission is approximately twice that of the optically thin emission. The effects for smearing represented in Figure 5a by the jagged curves are discussed later toward the end of this section.

Figure 5b shows relative brightness values for 100 km horizontal wavelength waves at z_{TRH}=85 km. Notice that a shallower viewing angle produces relative brightness amplitudes that vary from being marginally observable to completely unobservable for all phase speeds and viewing directions. A similar difference between forward and backward viewing is revealed for the 0-0 band emission, but the optically thin emission shows no difference, since both the foreground and background emission are included for calculations at z_{TRH}=85 km.

Figure 5c shows results of 1000 km horizontal wavelength waves at z_{TRH}=40 km. Here the optically thick 0-0 band emis-

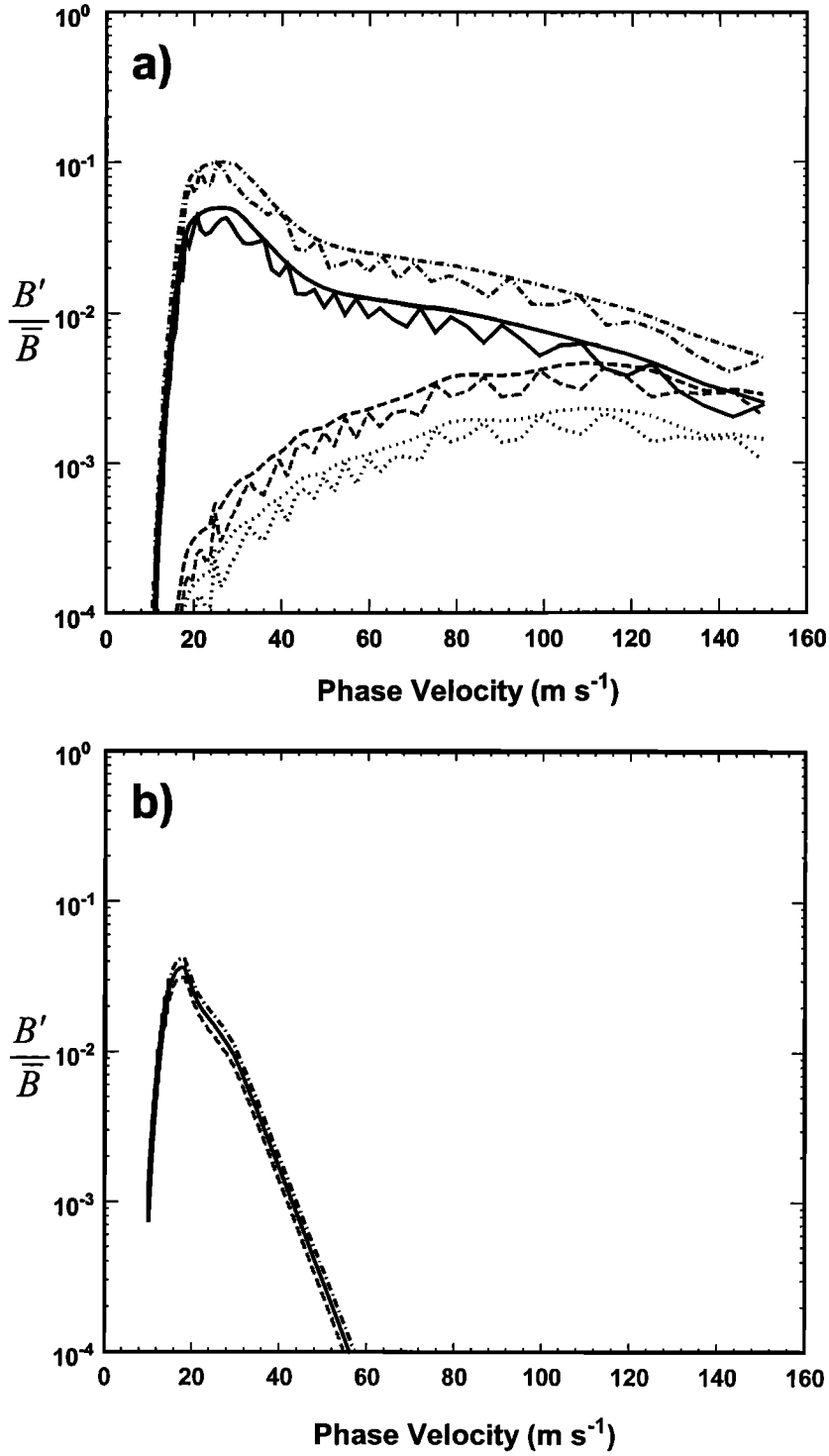

Figure 5. Integrated brightness perturbation amplitudes divided by mean amplitudes ($B'/\overline{B}$) plotted as a function of phase speed for waves used in our simulations. The solid curves correspond to 0-1 band (optically thin) emission for viewing in the backward direction along the line of sight, and the dotted curves correspond to the optically thin emission for forward viewing. The dashed curves correspond to the 0-0 band (optically thick) emission for forward viewing, and the dash-dotted curves correspond to the optically thick emission for backward viewing. Curves are plotted for (a) horizontal wavelength of 100 km and z_{TRH}= 40 km, (b) horizontal wavelength of 100 km and z_{TRH}= 85 km, (c) horizontal wavelength of 1000 km and z_{TRH}= 40 km, and (d) horizontal wavelength of 1000 km and z_{TRH}= 85 km. The effects of smearing are presented in Figure 5a for an integration time of 5.0 s. The smeared data appear as "jagged" curves that lie immediately below the model results.

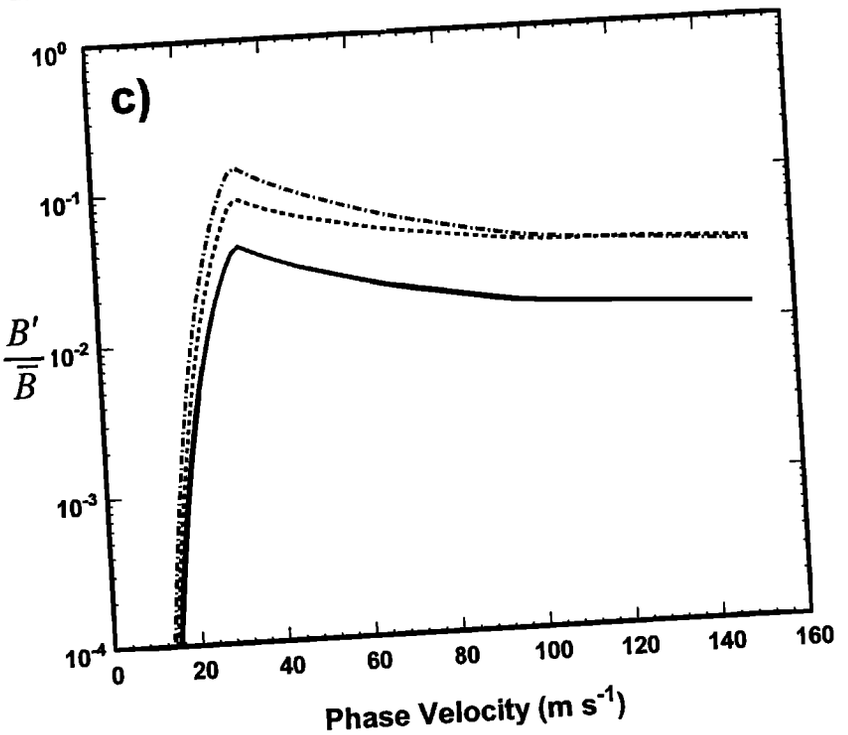

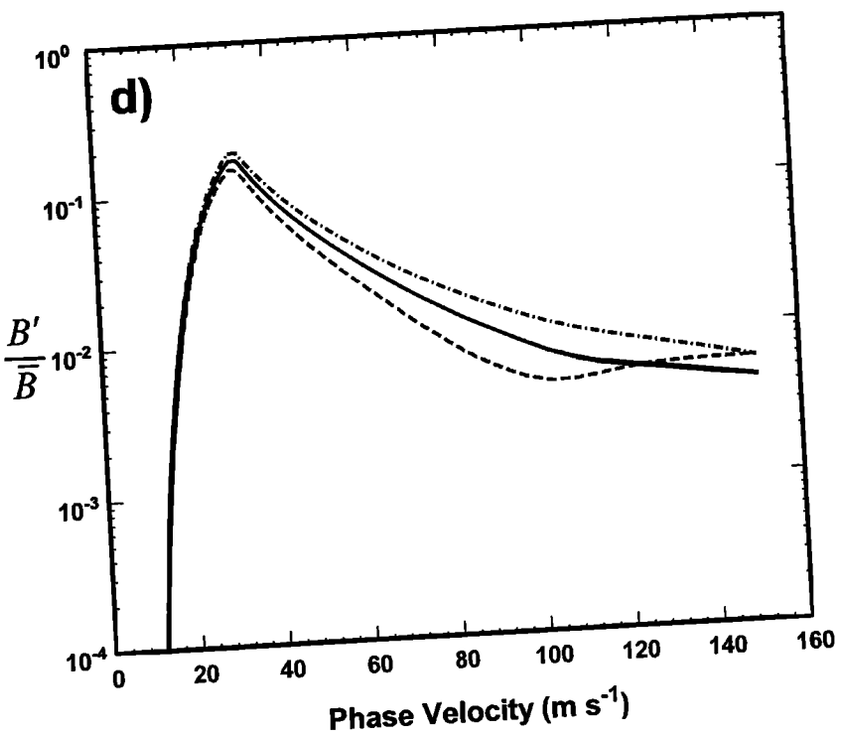

Figure 5. (continued)

sion is clearly observable in the phase velocity range 25-80 m s^{-1}. For larger horizontal wavelength the difference between forward and backward viewing is significantly smaller. The effect is largest for waves with phase speeds of the order of 30 m s^{-1}, and brightness values there can differ by almost a factor of 4, which should be observable. There is no difference in the optically thin 0-1 band emission between forward and backward viewing, and this emission is expected to be unobservable for the range of phase speeds considered. For the same 1000 km horizontal wavelength waves viewed at z_{TRH}=85 km (Figure 5d), the difference in brightness of the 0-0 band emission due to viewing direction is significantly enhanced for phase speeds greater than about 60 m s^{-1}, although the brightness amplitudes are not expected to be observable there. These waves (as viewed in the backward direction) are only predicted to be clearly observable in the phase velocity range 25-60 m s^{-1}. The optically thin 0-1 band emission brightness is the same for both forward and backward viewing

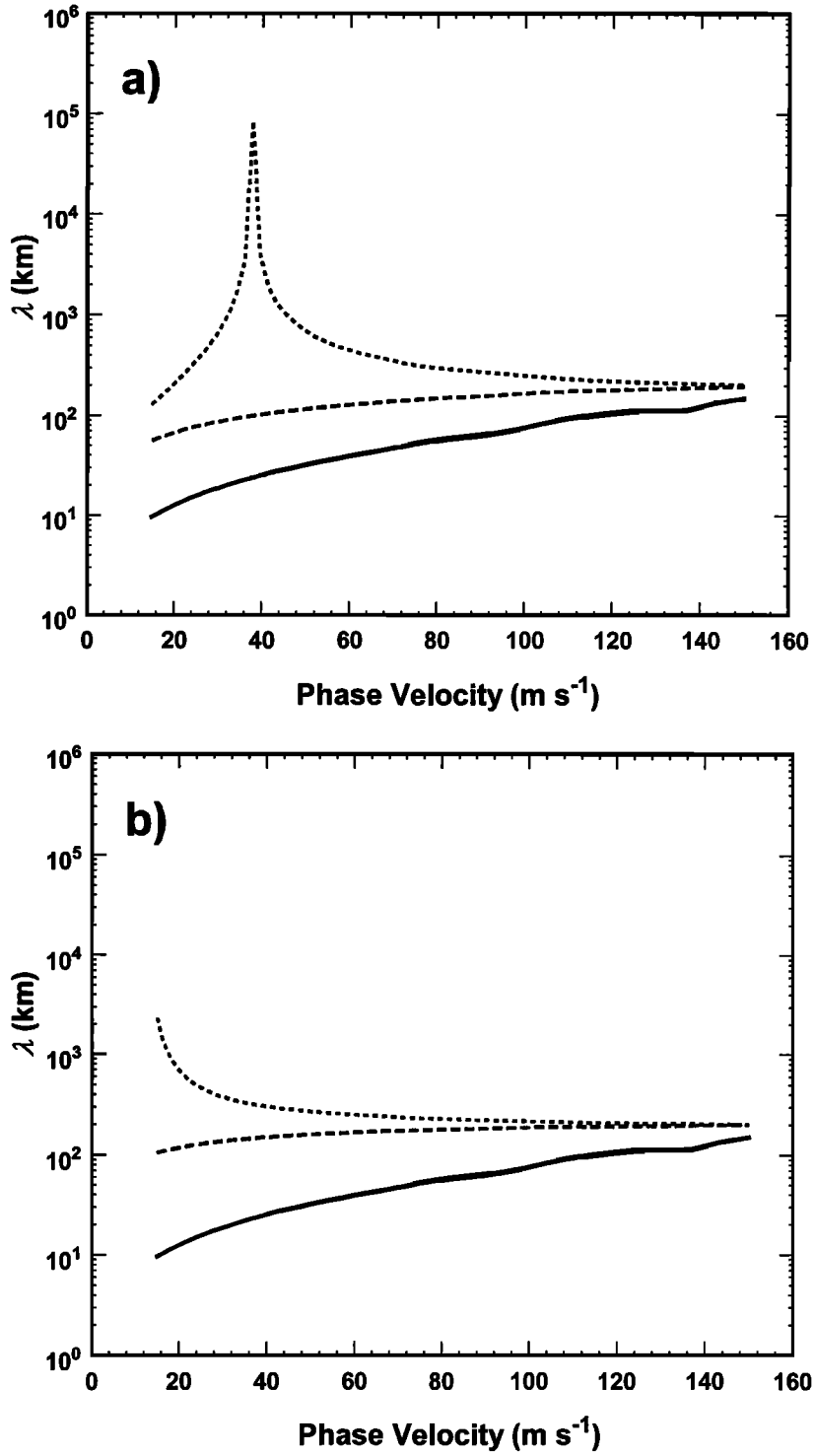

Figure 6. The apparent wavelength of the perturbation VER along the line of sight relative to the geometry of Figure 1 for forward (dashed curve) and backward (dotted curve) viewing plotted as a function of phase speed for the waves used in our simulations. The solid curve is the corresponding vertical wavelength. All wavelengths are calculated at an altitude roughly corresponding to the peak in the airglow emission (~91.5 km). Curves are plotted for (a) horizontal wavelength of 100 km and z_{TRH}= 40 km, (b) horizontal wavelength of 100 km and z_{TRH}= 85 km, (c) horizontal wavelength of 1000 km and z_{TRH}= 40 km, and (d) horizontal wavelength of 1000 km and z_{TRH}= 85 km.

because both regions lying on each side of the tangent ray point are included in the integration.

The geometric effect is illustrated in Figure 6 relative to the brightness curves shown in Figure 5. Here the dashed and dotted curves are the apparent wavelength in VER for forward and backward viewing, respectively, along the line of sight for a given tangent ray height. The solid curve is the corresponding vertical wavelength. For consistency, all values of

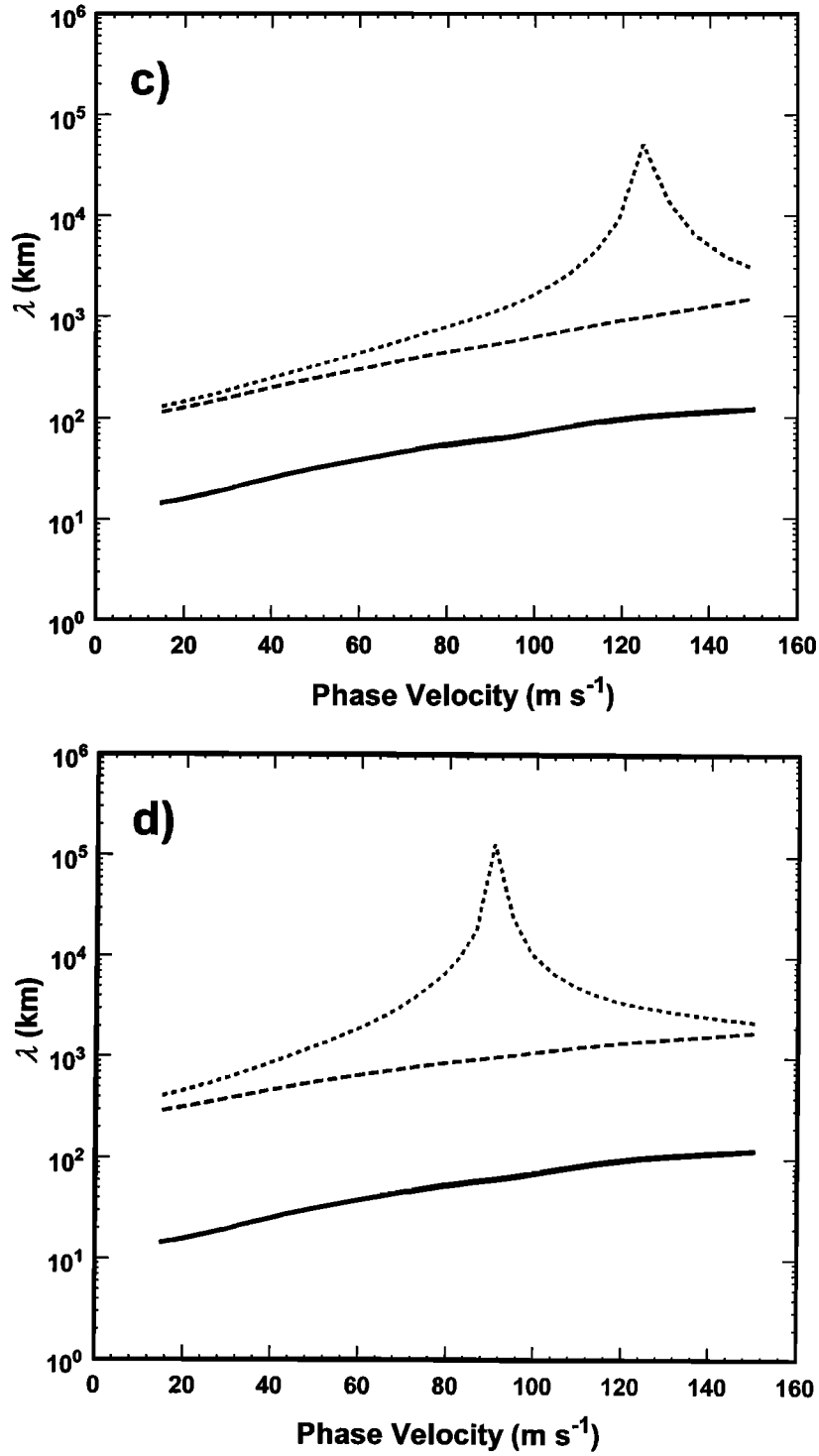

Figure 6. (continued)

the wavelength were calculated at an altitude that roughly corresponds to the peak in the airglow intensity (~91.5 km). Both the apparent and vertical wavelength increase with increasing phase velocity, which will be instrumental in diminishing the cancellation effect seen at small phase velocities.

As illustrated in Figure 5, the geometric effect is significant at lower phase speeds ($\leq$60 m s^{-1}). For higher phase speeds, the effect is less pronounced, and for very large phase speeds (>150 m s^{-1}) the difference between forward and backward viewing becomes negligible. For the four cases studied, the apparent wavelength for backward viewing is always larger than the apparent wavelength for forward viewing. The reduction in apparent wavelength for forward viewing along the line of sight leads to increased cancellation in the total integrated brightness due to effects of destructive interference. As the phase speed increases, so too does the apparent wavelength along the tangent ray. Eventually, the apparent wavelength exceeds a threshold value for which cancellation between different phases of VER fluctuations becomes negligible. Additionally, true vertical wavelengths increase

with increasing phase speed. Therefore, for the faster waves, brightness fluctuations for forward and backward viewing are approximately equal. Differences in apparent wavelength between forward and backward viewing will lead to differences in brightness for the slower waves.

For all cases in Figure 6, apparent wavelengths evaluated at ~91.5 km altitude along the line of sight for backward viewing become very large at certain phase speeds depending on the value of horizontal wavelength and tangent ray height. Very large values of apparent wavelength imply that the wave disturbances appear evanescent in the airglow, meaning that the VER fluctuations occurring at different positions along the tangent ray will be all in phase. This should minimize the effects of destructive interference between VER fluctuations occurring at different positions along the tangent ray, resulting in larger values of B'. For small phase speeds a locally constant phase means that the difference between apparent wavelengths for forward and backward viewing is a maximum, and we should expect a larger difference in brightness between the two viewing directions (compare Figures 5a and 6a and Figures 5d and 6d).

In Figure 5a the additional effect of finite integration time is illustrated as separate curves for forward and backward viewing and thick and thin emission. We only examine effects associated with instrumental smearing for the 100 km wavelength, z_{TRH} = 40 km case because these effects are the most significant for this particular wave. The averaging has been calculated at two separate integration times, 2.5 and 5.0 s, to mimic the data acquisition procedure for a typical optical device. A more complete analysis is left to the discussion section. The results obtained using a 2.5-s integration time are not significantly different from those obtained excluding smearing effects and so are not shown. For a 5-s integration (averaging) time, interpolated values of $B'/\overline{B}$ are smaller than the corresponding nonsmeared results. Additionally, the interpolation leads to jaggedness in the curves, as might be qualitatively expected for real measurements of the airglow when smearing effects are important. Overall, for values of $B'/\overline{B} \geq 0.1$, the effect of smearing is to reduce $B'/\overline{B}$ by about 20%. Therefore the 5-s smearing does not significantly affect the simulated brightness fluctuations for this case. As mentioned previously, the effect of smearing for longer horizontal wavelength waves (1000 km) becomes insignificant because during the 5-s measurement (integration) time, the tangent ray point will traverse a horizontal distance that is small compared with the horizontal wavelength. For example, for a satellite speed of 7.8 km s^{-1} and for z_{TRH} = 40 km, it would take ~140 s for the satellite to traverse a distance of 1000 km, which is significantly greater than the 5-s sampling time.

4. Discussion

As previously stated, we calculated and compared the brightness obtained (in the absence of waves) for nadir viewing and for sublimb viewing with a tangent ray height of 40 km and found that the brightness for the latter is a factor of approximately 16 times greater than that of the former. The implication is that space-based instruments viewing the sublimb will receive stronger signals than will nadir viewing instruments, allowing the use of shorter integration times. We have performed simulations of the O_2 atmospheric airglow emission, and we have considered integration times as long as 5 s. *Mende et al.* [1994] have performed topside measurements of the O_2 atmospheric nightglow (using an image-intensified CCD detector looking slightly below the limb), and typical exposures of 1 s allowed them to identify gravity waves having horizontal wavelengths of 50-100 km. Their broadband O_2 atmospheric measurements (which included a 10% contribution from the OH bands) had a typical brightness of 170 kR [see *Swenson et al.*, 1989]. *Ross et al.* [1992] imaged the UV O_2 Herzberg I emission (having a peak layer intensity of ~3 kR) using exposure times of 0.33 s and were able to infer a horizontal wavelength of about 15 km for the airglow structure. However, these were limb views and appear to have been obtained looking parallel to the phase fronts. Therefore the use of a 5-s integration time to obtain a single measurement appears modest. Our numerical simulations are based upon an assumed broadband measurement covering all of the O_2 atmospheric bands (for our assumed chemistry), and so the signal strength is strong, being ~40 kR and ~20 kR for the thin and thick emissions, respectively, for a tangent ray height of 40 km. (Note that our modeled 0-0 band brightness is smaller than the 0-1 band brightness, contrary to theory and observation. This is because we use the 0-1 band radiation transition probability to describe the 0-0 band emission, as discussed in section 2. This does not significantly affect our modeled relative brightness fluctuations, the subject of this paper, which are independent of absolute brightness. However, space-based measurements of the 0-0 band nightglow brightness by *Torr et al.* [1985] are ~200–500 kR for limb viewing.) If individual lines of a band were to be measured, much longer integration times would obviously be required to compensate for the reduced signal strength. Additionally, instruments can be operated in so-called "staring modes," wherein the same region of the airglow is sampled during the course of the satellite motion. This tends to reduce smearing effects.

We have assumed that an airglow relative brightness fluctuation of 5% due to a gravity wave would be observable. The airglow structures measured by *Mende et al.* [1994] had large (~20%) amplitudes, although their atmospheric emissions photometric imager (AEPI) experiment was able to detect airglow modulations when they were greater than 5–10%. However, as was stated by *Mende et al.* [1994], the AEPI imager was not designed originally for gravity wave-induced airglow detection, and an optimized instrument (with, for example, a bare CCD detector) would have a much higher dynamic range with a greater sensitivity to small-intensity variations. Airglow disturbances with amplitudes of 10-20% were also reported by *Ross et al.* [1992] using an intensified CCD imager. The exposure times for their images were 0.33 s. Clearly, the application of bare CCD detectors in future space-based experiments should permit the use of short integration times to enable the measurement of shorter-scale gravity waves.

Satellite-based studies of planetary-scale waves have revealed large longitudinal and latitudinal gradients of airglow VER. For example, *Ward et al.* [1996] determined the O I 5577 VER at 94 km altitude and obtained variations of ~50% over latitudinal distances as short as 3300 km, corresponding to about 5% variations per 330 km. This VER gradient is comparable to what might be expected of gravity waves. Careful removal of such large-scale features from airglow signals should be possible using fairly standard analysis procedures, which would leave behind the gravity wave signals

(perhaps with some distortion). As far as our modeling is concerned, we have not yet tackled the more complex but realistic case of gravity wave propagation and effects in an atmosphere having strong mean state (or slowly varying) gradients in the horizontal direction. In spite of this, the anisotropy effects discussed in this paper would still exist and should still permit the determination of propagation direction for waves having short enough vertical wavelength.

In this study we have employed the band-averaged optical depth (τ) given by *Wallace and Hunten* [1968]. Although our results would be affected by the use of different values of τ (such as those specific to the lines of a particular band being observed), the similarity in results obtained for the optically thin and optically thick emissions suggests that the effect would not be significant.

As discussed by *Hickey and Brown* [2000], increasing z_{TRH} had the effect of significantly reducing $B'/\overline{B}$ over the nominal values for the limited number of waves studied, implying that the waves would be difficult to observe. In support of this conclusion, in Figure 4 we have also presented the VER for a 100 km horizontal wavelength wave (phase velocity of 30 m s^{-1}) as a function of distance along the line of sight for z_{TRH}=85 km. In this case the number of oscillations significantly exceeds the number associated with z_{TRH}=40 km, leading to increased cancellation of wave effects and to decreased $B'/\overline{B}$ values (see Figures 4 and 5b).

For several waves at z_{TRH}= 85 km, this increased cancellation only occurs for small horizontal wavelengths (~100 km). For larger horizontal wavelengths (~1000 km), Figure 5d demonstrates that waves can be clearly observed within a significant range of phase velocities (25-60 m s^{-1}) at z_{TRH}=85 km, and additionally, the direction of propagation of these observable waves for the 0-0 band emission can be determined. Observations made at such shallow angles (large z_{TRH}) yield apparent wavelengths in the VER (within the entire velocity range) which are closer to the true horizontal wavelength of the wave (compare Figures 6a and 6b and Figures 6c and 6d). Thus, for short horizontal wavelengths, oscillations in the VER should be large when viewing at higher tangent ray heights and we should expect significant cancellation (see Figures 4 and 5b). For larger horizontal wavelengths, there will be fewer oscillations along the tangent ray and the waves should be clearly observable (see Figure 5d).

Nonlinear effects associated with the small scale-heights of the minor species involved in the airglow emission chemistry may be important for some gravity waves. We have performed calculations using a two-dimensional, time-dependent, nonlinear model [*Hickey et al.*, 2000] describing the interactions of gravity waves with the O_2 atmospheric airglow which confirm the results and conclusions presented here. This demonstrates that the results presented here are not a consequence of nonlinear effects, but instead are due to the geometry effects discussed earlier.

A consideration when viewing the same wave in the forward and backward viewing directions is the time delay between such observations. If it is too large, the characteristics of the wave may have changed enough to render the comparison meaningless. For a satellite height of 500 km, z_{TRH}=40 km, and an orbital period of 100 min, the time delay for observing the same volume element of the atmosphere for forward and backward viewing is approximately ~7 min. This is not large compared with typical gravity wave periods (~10 to 20 min or greater), so that it is reasonable to assume that the wave properties would not change significantly over this time interval.

We have not included height-dependent background winds in our analysis. Their effect will be to increase or decrease the local vertical wavelength over its windless value depending on the direction of wave propagation with respect to the winds, thus affecting the local tilt of the vertical phase fronts. Wind effects are more important for slower waves. In a windy background atmosphere it is the intrinsic direction of propagation (i.e., with respect to the moving atmosphere) that would be inferred by consideration of the anisotropy in airglow fluctuation brightness. These effects will be considered in a future study.

Finally, we have assumed that the satellite motion occurs in a plane perpendicular to the horizontal phase fronts of the waves. Our results maximize the difference between $B'/\overline{B}$ derived from forward and backward viewing. As the angle (θ) between the plane of the satellite motion and the phase fronts varies from $\pi/2$ (our nominal value) to 0, this difference will approach zero. For $\theta = 0$ or π, the determination of propagation direction as proposed here is no longer possible.

To test the sensitivity of our results to changes in θ, we have performed simulations for a wave of 100 km horizontal wavelength and phase velocity of 30 m s^{-1}. For the optically thin 0-1 band emission this set of wave parameters provides the largest difference between values of $B'/\overline{B}$ obtained for forward and backward viewing (see Figure 5a). Our results (not shown) demonstrate that as θ is decreased from $\pi/2$ to 0, the difference in $B'/\overline{B}$ (for different viewing azimuths) becomes negligible. However, the anisotropy in $B'/\overline{B}$ with respect to viewing azimuth remains strong for angles θ as small as 30°. $B'/\overline{B}$ also remains reasonably constant over this range, decreasing for angles smaller than 30°. Because we have assumed a cylindrical geometry in our calculations, these sensitivity test results will not be valid for smaller angles. However, the approach has allowed us to quantify (approximately) the range of angles θ for which the anisotropy effects may be expected to remain important. We very conservatively estimate the anisotropy to be strong for angles θ at least as small as 60°, which suggests the usefulness and general utility of the approach.

5. Conclusion

We have presented the results of simulations that show that the perturbation VER for atmospheric gravity waves having short vertical wavelengths is generally asymmetrical about the tangent ray point, producing an observational difference for satellites viewing gravity wave perturbations in airglow emissions in the forward and backward directions. These results imply that brightness fluctuations observed for the optically thick 0-0 band emission will always appear stronger for waves traveling toward the observer (the satellite). For some smaller-scale gravity waves, which are not expected to remain correlated over large horizontal distances, information useful for the interpretation of propagation direction could also be obtained using the optically thin 0-1 band emission. We have argued that for some waves, brightness fluctuation differences between forward and backward viewing directions should be observable and could be used to remove the 180° ambiguity in propagation direction for the waves. This will be a valuable tool for studying gravity waves from space because it is a method that does not rely on the simultaneous observations of

the waves using ground-based instruments. Although we have considered both the optically thick (0-0) and optically thin (0-1) bands of the O_2 atmospheric emission, our results show that the 0-0 band is better for resolving the 180° ambiguity in gravity wave propagation direction. We have also demonstrated that the waves studied should be clearly observable given the fact that a finite integration time is required for space-based measurements.

Finally, our proposed method for determining wave propagation direction works the best for waves having fairly short vertical wavelengths. Serendipitously, these are the same waves expected to be damping in the MLT region and significantly forcing the mean state. The method does not work as well for fast waves having large vertical wavelengths, but these are the waves expected to pass through the MLT region with little damping and therefore to have little impact on the energy and momentum budgets of the MLT region.

Acknowledgments. The authors are pleased to acknowledge support of this research by NASA grant NAGW-4762 to Clemson University. Discussions with Drs. John Meriwether and Gary Swenson are appreciated. The substantive comments of the referees are gratefully acknowledged.

Janet G. Luhmann thanks referees for their assistance in evaluating this work.

References

Armstrong, W. T., U.-P. Hoppe, G. G. Shepherd, and B. Solheim, Observations of gravity wave structure in O_2 (00) airglow measurements with the UARS-WINDII imager (abstract), *Eos Trans. AGU, 76*(46), Fall Meet. Suppl., F73, 1995.

Chamberlain, J. W., *Physics of the Aurora and Airglow, Classics Geophys. Se.,*, vol. 1, Washington, D. C., 1995.

Francis, S. H., Propagation of internal acoustic-gravity waves around a spherical Earth, *J. Geophys. Res., 77*, 4221-4226, 1972.

Fritts, D. C., R. C. Blanchard, and L. Coy, Gravity wave structure between 60 and 90 km inferred from Space Shuttle reentry data, *J. Atmos. Sci., 46*, 423-434, 1989.

Hays, P. B., G. Fall, B. Solheim, and G. G. Shepherd, Observing atmospheric waves from the UARS spacecraft (abstract), *Eos Trans. AGU, 75*(44), Fall Meet. Suppl., 111, 1994.

Hedin, A. E., Extension of the MSIS thermosphere model into the middle and lower atmosphere, *J. Geophys. Res., 96*, 1159-1172, 1991.

Hickey, M. P., and J. S. Brown, Resolving ambiguities in gravity wave propagation directions inherent in satellite observations: A simulation study, *Geophys. Res. Lett., 27*, 2901-2904, 2000.

Hickey, M. P., and R. L. Walterscheid, A note on gravity wave-driven volume emission rate weighted temperature perturbations inferred from O_2 atmospheric and O I 5577 airglow observations, *J. Geophys. Res., 104*, 4279-4286, 1999.

Hickey, M. P., R. L. Walterscheid, M. J. Taylor, W. Ward, G. Schubert, Q. Zhou, F. Garcia, M. C. Kelly, and G. G. Shepherd, Numerical simulations of gravity waves imaged over arecibo during the 10-day January 1993 campaign, *J. Geophys. Res., 102*, 11,475-11,489, 1997.

Hickey, M. P., M. J. Taylor, C. S. Gardner, and C. R. Gibbons, Full-wave modeling of small-scale gravity waves using airborne lidar and observations of the hawaiian airglow (ALOHA-93) O(^1S) images and coincident Na wind/temperature lidar measurements, *J. Geophys. Res., 103*, 6439-6453, 1998.

Hickey, M. P., R. L. Walterscheid, and P. G. Richards, Secular variations of atomic oxygen in the mesopause region induced by transient gravity wave packets, *Geophys. Res. Lett.*, in press, 2000.

Kafkalidis, J. F., W. R. Skinner, D. A. Gell, and P. B. Hays, Observations of gravity waves in the O_2 nightglow from space (abstract), *Eos Trans. AGU 77*(46), Fall Meet. Suppl., F105, 1996.

Mende, S. B., G. R. Swenson, S. P. Geller, and K. A. Spear, Topside observations of gravity waves, *Geophys. Res. Lett., 21*, 2283-2286, 1994.

Orlanski, I., and K. Bryan, Formation of the thermocline step structure by large-amplitude internal gravity waves, *J. Geophys. Res., 74*, 6975-6983, 1969.

Ross, M. N., A. B. Christensen, C. I. Meng, and J. F. Carbary, Structure in the UV nightglow observed from low Earth orbit, *Geophys. Res. Lett., 19*, 985-988, 1992.

Schubert, G., R. L. Walterscheid, M. P. Hickey, and C. A. Tepley, Theory and observations of gravity wave induced fluctuations in the OI (557.7 nm) airglow, *J. Geophys. Res., 104*, 14,915-14,924, 1999.

Swenson, G. R., S. B. Mende, and E. J. Llewellyn, Imaging observations of lower thermospheric O(^1S) and O_2 airglow emissions from STS 9: Implications of height variations, *J. Geophys. Res., 94*, 1417-1429, 1989.

Torr, M. R., D. G. Torr, and R. R. Laher, The O_2 atmospheric 0-0 band and related emissions at night from Spacelab 1, *J. Geophys. Res., 90*, 8525-8535, 1985.

Wallace, L., and D. M. Hunten, Dayglow of the oxygen A band, *J. Geophys. Res., 73*, 4813-4834, 1968.

Ward, W. E., D. Y. Wang, B. H. Solheim, and G. G. Shepherd, Observations of the two-day wave in WINDII data during January, 1993, *Geophys. Res. Lett., 23*, 2923-2926, 1996.

J. S. Brown and M. P. Hickey, Department of Physics and Astronomy, Clemson University, Clemson, South Carolina 29634-0978. (jsbrown@ces.clemson.edu; hickey@hubcap.clemson.edu.)

(Received July 11, 2000; revised September 18, 2000;
accepted September 19, 2000.)